JOURNAL OF APPLIED ELECTROCHEMISTRY 15 (1985) 351–363

Studies on chemically precipitated Mn(IV) oxides. IV. Effect of dopants/impurities on the discharge behaviour of chemical manganese dioxide in alkaline medium and the applicability of Atlung–Jacobsen model to the $(MnO_2)_{1-r}(MnOOH)_r$ system

JULIO B. FERNANDES, BUQUI D. DESAI, V. N. KAMAT DALAL

Department of Chemistry, Centre of Postgraduate Instruction & Research, Panaji, Goa 403 001, India

Received 25 April 1984; revised 9 July 1984

Manganese (IV) oxides are synthesized by chlorate oxidation of Mn(II) salts containing varying amounts of Fe^{3+} ions. An Mn(IV) oxide containing MoO_3 is also synthesized. All the oxides are characterized by chemical analyses, X-ray, infrared and magnetic susceptibility studies. It is observed that increasing the amount of Fe^{3+} in the Mn(II) solution favours the formation of the gamma-phase. The catalytic and electrochemical activity of the dioxides are evaluated and discussed *vis-à-vis* their structural factors. The structure and activity are further discussed in the light of the Atlung–Jacobsen model and the recent electrochemical reduction mechanism of Maskell, Shaw and Tye.

1. Introduction

Manganese dioxides doped with certain cations are known to exhibit different structural behaviour [1, 2] and battery activity [3]. Some workers [4, 5] have studied the effect of doping manganese dioxides with cations such as Li^{1+}, Cr^{3+}, Th^{4+}, etc., on their isoelectric point. Electrolytically prepared MnO_2 containing Fe^{3+} is reported to give good battery performance [6]. MoO_3-doped MnO_2 cathodes obtained by heating $Mn(NO_3)_2$ and containing less than 0.1% MoO_3 reportedly exhibit superior discharge performance in a reserve primary battery [7]. The present investigation is aimed at studying the influence of some of the dopants on the crystal structure of chemical manganese dioxide (CMD). The discharge behaviour of CMD and doped CMD in alkaline medium is examined on the basis of the Atlung–Jacobsen model which treats MnO_2 as an insertion electrode analogous to the Li–TiS_2 electrode. An attempt is made to focus attention on the comparison between the theoretically calculated potential curves with those obtained from the experimental values. The deviations observed are explained tentatively on the basis of the formation of a new compound in the case of chemical manganese dioxides in general.

2. Experimental details

The reagents $MnCl_2 \cdot 4H_2O$, $Fe(NO_3) \cdot 9H_2O$ and MoO_3 used in this work were BDH Analar grade. $KClO_3$ and $NaClO_3$ were pro analysis E. Merck. Crude Mn(II) chloride and sulphate solutions were prepared from a natural ore from Sanvordem mines, Goa, India; the ore having the following composition: Mn 50.4%, MnO_2 79.1%, Fe_2O_3 10.4% and SiO_2 9.3% as the major constituents. $MnCl_2$ was obtained by direct leaching of the ore in the minimum amount of concentrated HCl. $MnSO_4$ was obtained by disproportionation of the reduced ore in 10% H_2SO_4. The experimental details involved in the preparation of these salts and their subsequent oxidation to the dioxides by the chlorate method are described elsewhere [8, 9].

The dioxides were characterized by chemical

0021–891X/85 $03.00 + .12

analyses, X-ray diffraction and infrared spectroscopy. The H^+ ion exchange capacity was determined as described earlier [9]. The discharge characteristics were evaluated in 9M KOH solution at 1 mA constant current discharge using a modified method of Kozawa [10]. Room temperature magnetic susceptibility measurements were made by the Gouy method [11].

The actual quantities of the reagents used in the syntheses as well as the chemical analyses and formulae of the dioxides are presented in Table 1a. For ready reference similar description of some of the samples reported earlier is presented in Table 1b.

3. Results and discussion

3.1. *Synthesis, chemical analysis, X-ray and infrared studies*

The manganese dioxide samples B_1, B_2, B_3 and B_4 were synthesized under identical experimental conditions as those obtained from pure Mn(II) salts except that the Mn(II) salts used were obtained from a natural ore and contained Fe^{3+} as a major impurity. A comparison of their chemical composition (Table 1a) with the previously reported samples (Table 1b) indicated no notable changes in MnO_2 content. In fact on average a slight increase in combined water content was observed. This was reflected in the higher values of m in the chemical formulae. Further, samples B_1 and A_2 were identically synthesized, i.e. by the oxidation of $MnCl_2$, $KClO_3$ being added in two equal instalments. Similarly the syntheses of A_2 and B_5 were identical, $NaClO_3$ being added in one undivided lot. In all the above cases, the γ-phase of MnO_2 was obtained, as is evident from the X-ray diffraction data (Table 2a). Samples B_3 and B_4 were obtained by the oxidation of crude $MnSO_4$ salts by $KClO_3$ and $NaClO_3$ respectively. Their d, I/I_0 values (Table 2a) indicate that they belong to the α-crystallographic form and are identical to A_6 and A_7, the latter being similarly synthesized from pure $MnSO_4$.

Group C samples C_1, C_2 and C_3 were all precipitated using $KClO_3$, this being added in one undivided lot to $MnCl_2$ solution containing varying amounts of $Fe(NO_3)_3$. The experimental conditions were identical to those for sample A_1. The chemical compositions and amounts of Fe^{3+} doped are presented in Table 1a.

The X-ray diffraction data indicate that samples A_1 [9], C_1 and C_2 all belong to the mixed crystal phase. The presence of Fe^{3+}, however, seems to favour the formation of the γ-phase. A comparison of the intensities of the $d = 0.163$ nm peak in C_1 and A_1 indicates this. This is usually a ⟨1 0 0⟩ intensity peak of the γ-MnO_2 samples prepared in this investigation. The relative intensities of this peak in A_1 and C_1 are 65 and 80, respectively. The sample C_3 has a greater Fe^{3+} content (% $Fe^{3+} = 1.52$) compared to C_1 (% $Fe^{3+} = 0.78$). C_2, in addition, shows a typical γ-MnO_2 peak at $d = 0.405$ nm ($I/I_0 = 42$). Strangely enough the ⟨1 0 0⟩ intensity peak of C_2 is at $d = 0.68$ nm while all the other α-MnO_2 samples and α, γ-mixed crystal phase types have their maximum reflection around $d = 0.239$ nm. That the Fe^{3+} content favours the formation of γ-phase is confirmed by the X-ray diffraction data of sample C_3 (Table 2b). It has the highest Fe^{3+} content (% $Fe^{3+} = 3.88$) and d, I/I_0 values indicate that it is a pure γ-MnO_2. Sample C_4 is also precipitated in an identical manner as above but in the presence of a small amount of MoO_3 instead of Fe^{3+}. Its diffraction data indicate that it is a pure γ-MnO_2, indicating the favourable effect of Mo^{6+} on the formation of the γ-crystal phase. All these samples show increased combined water content compared to the undoped samples (Table 1a). Their MnO_2 content, however, is slightly less.

The infrared spectra of these MnO_2 samples are depicted in Fig. 1 and their absorption frequencies are presented in Table 3. In the earlier investigation [9] the characterization of the dioxides from their absorption frequency data and the shapes of the ir absorption bands were discussed in detail. Thus the γ-MnO_2 samples B_1, B_2, C_3 and C_4 show the characteristic broad absorption bands in the frequency range 400–750 cm^{-1}. They are also marked by the absorptions around 3400 and 1600 cm^{-1} corresponding to the stretching and bending vibrational modes, respectively of the OH groups present in the dioxide structures. The α-MnO_2 samples B_3 and B_4 as well as the α, γ-mixed crystal phase types are marked by their absorptions around 480, 530 and 700 cm^{-1}.

Samples B_3 and B_4, while exhibiting absorption around 1600 cm^{-1} do not show an absorption

Table 1. (a) Preparation, chemical analyses and formulae of the manganese dioxides

Sample	*Quantities of reagents used*	*MnO_2 (%)*	*Mn (%)*	*Fe (%)*	x *in* MnO_x	*Combined water* (y) (%)	*Formula* $(MnO_2)_{2n-3}(MnOOH)_{4-2n}mH_2O$
B_1	80 g $KClO_3$ in two equal instalments and crude $MnCl_2$ solution containing 16 g Mn	89.9	59.1	0.64	1.962	3.5	$(MnO_2)_{0.96}(MnOOH)_{0.04}0.16\,H_2O$
B_2	69.5 g $NaClO_3$ and crude $MnCl_2$ 16 g solution containing Mn	91.8	59.8	1.13	1.971	4.5	$(MnO_2)_{0.97}(MnOOH)_{0.03}0.21\,H_2O$
B_3	77 g $KClO_3$ and crude $MnSO_4$ solution containing 16 g Mn	86.3	57.7	0.33	1.945	2.7	$(MnO_2)_{0.94}(MnOOH)_{0.06}0.11\,H_2O$
B_4	67 g $NaClO_3$ and crude $MnSO_4$ as above	90.8	60.4	0.41	1.950	3.2	$(MnO_2)_{0.95}(MnOOH)_{0.05}0.13\,H_2O$
C_1	80 g $KClO_3$ and 57 g $MnCl_2$ containing 3.4 g $Fe(NO_3)_3 \cdot 9H_2O$	87.6	57.0	0.78	1.971	4.0	$(MnO_2)_{0.97}(MnOOH)_{0.03}0.19\,H_2O$
C_2	80 g $KClO_3$ and 57 g $MnCl_2$ containing 8 g $Fe(NO_3)_3 \cdot 9H_2O$	86.7	57.0	1.52	1.962	5.0	$(MnO_2)_{0.96}(MnOOH)_{0.04}0.23\,H_2O$
C_3	80 g $KClO_3$ and 57 g $MnCl_2$ containing 30 g $Fe(NO_3)_3 \cdot 9H_2O$	85.8	57.0	3.88	1.950	4.5	$(MnO_2)_{0.95}(MnOOH)_{0.05}0.21\,H_2O$
C_4	80g $KClO_3$ and 57 g $MnCl_2$ containing 220 mg MoO_3	91.4	59.1	% MoO_3 = 0.8	1.980	3.7	$(MnO_2)_{0.98}(MnOOH)_{0.02}0.18\,H_2O$

Table 1. (b) Preparation, chemical analyses and formulae of the manganese dioxides [10]

Sample	*Quantities of reagents used*	MnO_2 (%)	*Mn* (%)	x *in* MnO_x	*Combined water* (y) (%)	*Formula* $(MnO_2)_{2n-3}(MnOOH)_{4-2n}mH_2O$
A_1	80 g $KClO_3$ and 57 g $MnCl_2$ solution	90.1	59.1	1.965	3.0	$(MnO_2)_{0.96}(MnOOH)_{0.035}0.13\,H_2O$
A_2	80 g $KClO_3$ in two equal instalments and 57 g $MnCl_2$	91.7	59.7	1.970	2.5	$(MnO_2)_{0.97}(MnOOH)_{0.03}0.11\,H_2O$
A_5	69.5 g $NaClO_3$ and 57 g $MnCl_2$	93.6	60.4	1.979	4.5	$(MnO_2)_{0.98}(MnOOH)_{0.021}0.21\,H_2O$
A_6	77 g $KClO_3$ and 64.2 g $MnSO_4$	85.8	57.7	1.939	2.5	$(MnO_2)_{0.94}(MnOOH)_{0.07}0.09\,H_2O$
A_7	67 g $NaClO_3$ and 64.2 g $MnSO_4$	90.7	60.4	1.949	3.1	$(MnO_2)_{0.95}(MnOOH)_{0.05}0.13\,H_2O$

around 1600 cm^{-1} corresponding to the O–H bending vibrational mode. This was expected in the light of earlier observations [9] for α-MnO_2 samples A_6 and A_7. Samples C_1 and C_2, α, γ-mixed phase types, however, show slight absorption around 1600 cm^{-1} which was anticipated in view of the presence of the γ-phase. The above observations once again emphasize the convenience and simplicity of infrared spectral analysis in characterizing manganese dioxide crystal phases.

3.2. *Magnetic susceptibility studies*

The room temperature paramagnetic susceptibility values (χ) of the samples are presented in Table 4. The values for the undoped samples reported earlier [11], in general, follow the trend $\gamma \geqslant \alpha > \beta$-$MnO_2$. The γ-$MnO_2$ samples B_1 and B_2, which have Fe^{3+} as a major impurity, show higher susceptibility values than the similarly prepared γ-MnO_2 samples A_2 and A_5 which do not contain

Table 2. (a) X-Ray powder diffraction data of the manganese dioxides

B_1 (γ)			B_2 (γ)			B_3 (α)			B_4 (α)		
d (*nm*)	I/I_0	*hkl*	d (*nm*)	I/I_0	*hkl*	d (*nm*)	I/I_0	*hkl*	d (*nm*)	I/I_0	*hkl*
						7.20	31	1 1 0	7.00	29	1 1 0
						5.10	30	2 0 0	4.90	18	2 0 0
0.406	very very weak	1 1 0	4.06	12	1 1 0						
						3.17	64	3 1 0	3.12	22	3 1 0
0.242	20	0 2 1	2.41	58	0 2 1	2.40	100	4 1 0	2.36	100	4 1 0
0.2112	14	1 2 1	2.12	87	1 2 1	2.18	47	3 0 1	2.16	12	3 0 1
						1.84	50	4 1 1	1.83	30	4 1 1
0.164	100	2 2 1	1.63	100	2 2 1	1.65	41	6 0 0	1.64	30	6 0 0
						1.55	25	5 4 0	1.54	12	5 4 0
0.143	7	0 0 2	1.43	20	0 0 2	1.445	40	6 0 1	1.43	27	6 0 1
			1.394	19	1 6 1	1.362	20	–	1.36	10	–
Orthorhombic a = 0.4460 nm b = 0.9082 nm c = 0.2860 nm			Orthorhombic a = 0.4426 nm b = 0.8953 nm c = 0.2860 nm			Tetragonal $a = b$ = 1.002 nm c = 0.2858 nm			Tetragonal $a = b$ = 0.9833 nm c = 0.2884 nm		

Table 2. (b) X-Ray powder diffraction data of the manganese dioxides

C_1 (α, γ)			C_2 (α, γ)			C_3 (γ)			C_4 (γ)		
d (*nm*)	I/I_0	*hkl*	d (*nm*)	I/I_0	*hkl*	d (*nm*)	I/I_0	*hkl*	d (*nm*)	I/I_0	*hkl*
0.680	43	1 1 0	0.680	100	1 1 0						
0.485	64	2 0 0	0.490	80	2 0 0						
			0.405	42	–	0.399	45	1 1 0	0.410	12	1 1 0
0.308	75	3 1 0	0.308	54	3 1 0						
0.239	100	4 1 0	0.238	90	4 1 0	0.242	50	0 2 1	0.242	90	0 2 1
0.214	51	3 0 1	0.214	27	3 0 1	0.212	36	1 2 1	0.212	75	1 2 1
0.181	27	4 1 1	0.181	62	4 1 1						
0.163	80	6 0 0	0.163	62	6 0 0	0.164	100	2 2 1	0.164	100	2 2 1
0.1525	22	5 4 0	0.1545	28	5 4 0						
						0.147	36	0 0 2	0.143	33	0 0 2
						0.139	15	0 2 2	0.140	22	0 2 2
0.1341	40	–									
Tetragonal			Tetragonal			Orthorhombic			Orthorhombic		
$a = b = 0.9742$ nm			$a = b = 0.9774$ nm			$a = 0.4485$ nm			$a = 0.4459$ nm		
$c = 0.2937$ nm			$c = 0.2830$ nm			$b = 0.8470$ nm			$b = 0.9032$ nm		
						$c = 0.2950$ nm			$c = 0.286$ nm		

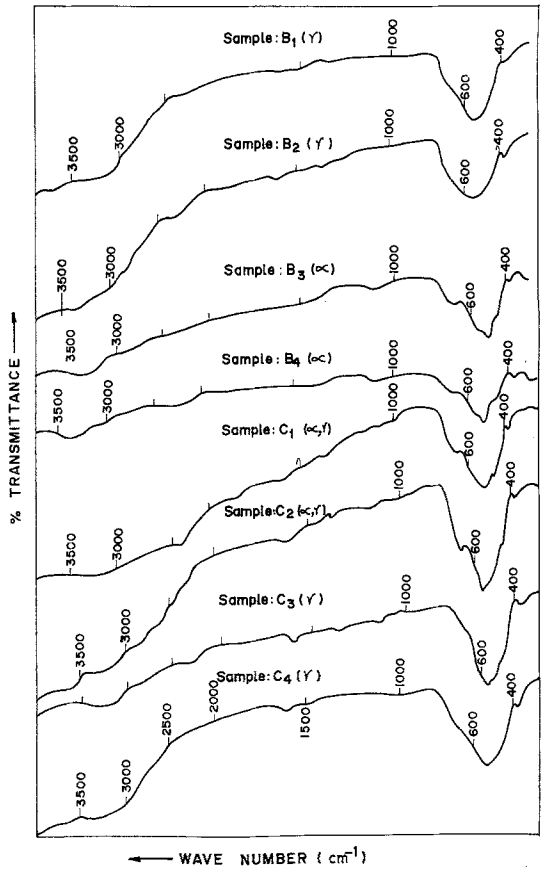

Fig. 1. Infrared spectra of the manganese dioxides.

Fe^{3+} as they were obtained from pure MnO_2 salts. The susceptibility values of the α-MnO_2 samples B_3, B_4, A_6 and A_7, however, are more or less identical.

The Fe^{3+}-doped samples C_1, C_2 and C_3 show a considerable increase in the susceptibility values. This is evident especially when one compares the values of C_1 and C_2 with that of sample A_1 as the latter has the identical crystal structure α, γ-phase. It has been reported [26] that the presence of impurities increases the susceptibility of the dioxides. In that case one would expect an almost linear increase in the χ values from C_1 to C_2 to C_3 since the Fe^{3+} content progressively increases in that order (see Table 1a). C_3 is, therefore, expected to show the highest values of susceptibility not only because of increased Fe^{3+} content but also due to the fact that it belongs to the γ-phase. It has already been shown [11] that the γ-crystal phases of MnO_2 have at least equal if not higher values of susceptibility than the α-MnO_2 samples as well as the α, γ-mixed crystal phase types. The fact remains, however, that sample C_2 (a mixed crystal phase like A_1 or C_1) shows the highest χ values. This leads one to believe that factors such as the impurity content and the differences in crystal phase types alone are not sufficient to explain the magnetic behaviour of manganese

Table 3. Infrared absorption frequency data of the manganese dioxides in relation to crystal phase

Sample	*Infrared absorption frequencies* (cm^{-1})												*Crystal phase*
B_1	3000–3500	1600	1470	1375					400–700		380		γ
B_2	3200–3500 2300	1610		1375					400–750		380		γ
B_3	3100–3550	–	1400		1100			705	530	475	380		α
B_4	3100–3600 2100	–		1350	1100			710	530	480	380		α
C_1	2900–3500 2300 1850	1600	1450	1375	1100	1000		690	535	470	380		α, γ
C_2	3100–3500	1600	1450	1375	1100	1000	930	690	570	450	380		α, γ
C_3	3100–3500 2300 1780	1620		1375	1150				400–740		380		γ
C_4	2900–3500	1600	1480						400–800		380		γ

dioxide. What seems to be required is a refinement of the structure of the doped MnO_2 and the determination of the oxidation state of the metals present on the surface as well as in the bulk. This type of study will reveal whether the dopant forms a solid solution or is present as a separate phase.

It is rather tempting to surmise that C_2, which has an unusual diffraction pattern might have Fe_2O_3 as a separate phase. With this view in mind a detailed low temperature magnetic susceptibility study has already been undertaken, the details of which will be communicated in due course.

3.3. *Study of chemical activity*

The H^+ ion exchange capacity measured in terms of volumes of thiosulphate is believed to give a fair measure of the relative chemical or catalytic activity of the manganese dioxides [8]. The reaction involves the liberation of I_2 from KI after the exchange of H^+ from the O–H groups of the dioxides by K^+ ions. The I_2 liberated is titrated against 0.01 M $Na_2S_2O_3$ solution.

The number of OH groups in the active dioxides is represented by the value of $(4-2n)$ in their chemical formulae (Tables 1a and b). It is seen that the number of OH groups in the dioxides, in general, follows the trend $\alpha > (\alpha, \gamma) > \gamma$-$MnO_2$. This may explain the increase in the H^+ exchange capacity of the different crystalline phases which follow the same order (compare the volumes of thiosulphate, Table 4). The situation, however, is different when a comparison of exchange capacity is made within a particular crystal phase-type. Thus, among the γ-MnO_2 samples the exchange capacity of A_2 is appreciably less than that of A_5 even though the $(4-2n)$ value of A_2 is significantly greater. The same holds good when a comparison is made within the α-MnO_2 samples A_6 and A_7 or B_3 and B_4. This may imply that all the OH groups in the dioxides are not necessarily exchangeable. Investigations of Brenet *et al.* [12, 13] indicate that the groutite (α-MnOOH) type oxyhydroxides do not have acidic OH groups, otherwise these compounds would show maximum H^+ ion exchange capacity. According to the struc-

Table 4. Magnetic susceptibilities and catalytic activity in terms of volumes of $S_2O_3^{-2}$ of the manganese dioxides in relation to crystal phase

Sample	B_1	B_2	B_3	B_4	C_1	C_2	C_3	C_4	A_1^*	A_2	A_5	A_6	A_7
Crystal phase	γ	γ	α	α	(α, γ)	(α, γ)	γ	γ	(α, γ)	γ	γ	α	α
$\chi \times 10^{-6}$ g^{-1} (at 25° C)	38.9	39.1	32.7	33.8	38.6	54.6	41.0	38.4	34.4	36.8	37.9	33.1	35.3
Volume of $S_2O_3^{-2}$ (ml)	28	25	63	71	53	57	40	42	51	18	29	61	68
b/c	3.17	3.13	3.5	3.4	3.31	3.45	2.87	3.17	3.37	3.13	3.17	3.38	3.42

* The data of the samples A_1, A_2, A_5, A_6 and A_7 have already been reported [9, 11] and are presented here for comparison.

ture of groutite given by Dent-Glasser and Ingram [14] the covalently bonded hydrogen of an O(2) oxygen in a particular octahedron is also bonded to another O(1) of another octahedron across a tunnel through a hydrogen bond. The hydrogens bonded in the above manner seem to be stabilized in the structure and are, therefore, non-acidic or non-exchangeable. It seems reasonable to conclude that only those hydrogens bonded otherwise or non-hydrogen bonded ones should be exchangeable. All this seems to suggest that in a parent dioxide structure the OH groups are of two types: exchangeable and non-exchangeable. Since α-MnO_2 samples exhibit greater exchange capacity than the γ-forms it appears that most of the hydrogens in the former are bonded otherwise and hence, more exchangeable. This seems reasonable since in the parent or unreduced α-MnO_2 the hydrogen bond formation should be less feasible, as the electrostatic forces for the formation of hydrogen bond should operate across a larger (2 x 2) tunnel and are, therefore, weaker as against the forces across (1 x 2) tunnels in the Ramsdellite type structures. While this may explain the relatively higher exchange capacity of the α-forms, why the exchange capacity is inversely related to the number of OH groups within a crystal phase is still not very clear.

It is quite possible that within a particular crystal phase type the exchange capacity of the exchangeable OH groups is governed by the relative O--H bond strengths.

It is seen from Table 4, that within any crystal phase, the Fe^{3+} containing samples have higher thiosulphate volumes compared to the undoped Group A samples, indicating that the former have relatively high catalytic activity. Since these samples also have high χ values the metal–oxygen bond length should also be comparatively greater. In general a slight increase in the b/c ratio is observed for Fe^{3+}-doped samples [8] hinting at slight lattice dilation; C_3, however, does not seem to fit the pattern. Further, the earlier results [11] regarding the relationship between b/c and volumes of thiosulphate should lend support to the hypothesis of the lengthening of the metal–oxygen bond and the consequent increase in the χ values.

3.4. *The discharge characteristics*

The discharge curves of some of the manganese dioxides evaluated in 9M KOH solution through a 1 mA constant current are shown in Fig. 2. The results are summarized in Table 5. The usable energy values, hereinafter referred to as E_u, are given in the last column of Table 5. These values are considered to give a fair measure of the relative electrochemical or battery activity of the samples [10].

Comparison of the E_u values of these MnO_2 immediately indicate that the Fe^{3+} containing γ-MnO_2 samples B_1, B_2 and C_3 are electrochemically less active than the samples A_2 or A_5 which are identically synthesized in the absence of any Fe^{3+}. Further, comparison of E_u values of the $KClO_3$ oxidized samples A_2. B_1 and C_3 (% Fe = 3.88) indicate that the electrochemical activity of the samples decreases with the increase in Fe content. This is rather interesting in the light of some previous work [6] in which electrolytic MnO_2 containing Fe^{3+} shows improved battery activity.

Table 5. Discharge characteristics of the manganese dioxides in 9M KOH solution and at a constant current of 1 mA

Sample	*Crystal phase*	*Open circuit voltage OCV (V)*		*Closed circuit voltage (CCV) at 5 mA h (V)*	*Polarisation η (mV)*			*Discharge time at 1.0 V cut-off (h)*	*Usable Energy E_u ($J\,g^{-1}$)*
		Initial	*At 5 mA h*		*At 5 mA h*	*At 13 mA h*	*At 21 mA h*		
B_1	γ	1.575	1.43	1.415	15	5	35	26.5	232
B_2	γ	1.575	1.44	1.425	15	5	30	26.0	252
C_3	γ	1.60	1.43	1.42	10	50	–	27.0	210
C_4	γ	1.58	1.425	1.420	5	25	40	26.5	209
A_2 [10]	γ	1.57	1.435	1.420	15	15	25	25.5	258
A_5 [10]	γ	1.665	1.475	1.44	35	15	20	27.0	288

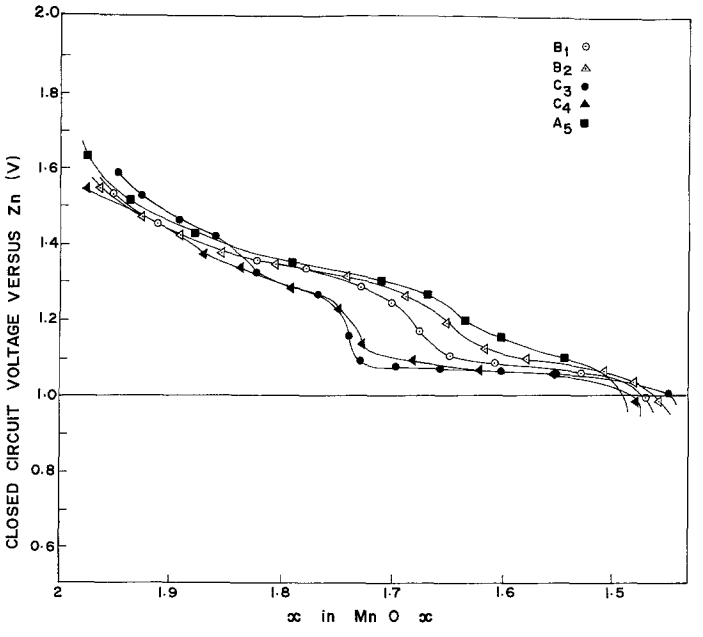

Fig. 2. Discharge curves of the manganese dioxides in 9M KOH solution and at a constant current of 1 mA.

It is seen from the discharge curves that there is a sudden collapse of the phase breadth of homogeneous reduction of C_3 around $x = 1.73$ of MnO_x. After this the reduction is probably heterogeneous as the discharge proceeds more or less at a constant voltage till the cut-off voltage of 1 V. This would also imply that sample B_1 which contains a lower amount of Fe^{3+} than C_3 shows a greater phase breadth of homogeneous reduction up to about $x = 1.64$. The above results clearly indicate that the presence of Fe^{3+} in the crystal lattice of a chemically precipitated MnO_2 is detrimental to its discharge performance. It is interesting to note, however, that the doped samples, in general, show lower cathodic polarization than the undoped samples (Table 5). There is also no significant difference in the discharge duration of the various dioxides (at 1 V cut-off).

The discharge characteristics as well as the shapes of the discharge curves of the Fe^{3+} doped γ-MnO_2 sample C_3 and MoO_3 doped γ-MnO_2 sample C_4 (% $MoO_3 = 0.8$) are almost identical. Both have almost the same value of E_u, i.e. 209 J g^{-1}, which is appreciably less than the similarly synthesized undoped γ-MnO_2 sample A_2 ($E_u = 258$ J g^{-1}). Incidentally, it has been reported [7] that the MoO_3 doped cathodes containing less than 0.1% MoO_3 show improved discharge performance. This is, however, not the case with C_4. Probably MoO_3 improves the discharge performance of a β-MnO_2 and has an adverse effect when present in a chemically precipiated γ-MnO_2.

3.5. *Applicability of the Atlung-Jocobsen model*

It is well known that the electrochemical reduction of a γ-MnO_2 takes place by proton–electron insertion in the MnO_2 lattice as envisaged in the following reaction:

$$MnO_2 + H^+ + e \rightleftharpoons MnOOH$$

According to Maskell, Shaw and Tye [15] the filling of either protons or electrons in the lattice takes place differently in the ranges above and below $MnO_{1.75}$. Above $MnO_{1.75}$ it is suggested that the inserted electron becomes delocalized between Mn^{4+} adjacent ions and the protons are involved in bond formation (covalent and hydrogen bonding) with oxygens in the O(2) coordination, i.e. pyramidal coordination with respect to Mn-atoms. In the second half, i.e. between $MnO_{1.75}$ to $MnO_{1.5}$, either the electron is associated with a single Mn^{4+} ion or the proton is convalently bonded to an oxygen in O(2) coordination and hydrogen-bonded to another in O(1), i.e. oxygen atoms in planar coordination with respect to Mn-atoms. Using the Nernst

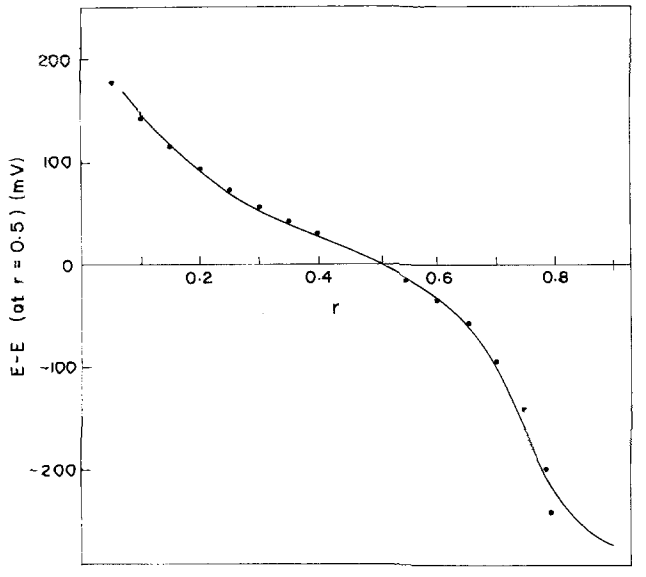

Fig. 3. Calculated and observed MnO_2 potential curves of IC_2; —— – observed, ... – calculated ($\alpha = 0.25$).

relation for the above electrochemical reduction process it follows that:

$$E = E^0 + RT/F \ln \frac{a_{MnO_2} a_{H^+} a_e}{a_{MnOOH}} \quad (1)$$

Over the years considerable attention has been paid to predicting the electrode potential of the system $MnO_2/MnOOH$ [16–19], but these attempts have met with limited success. Maskell, Shaw and Tye [20, 21] obtained good agreement between the observed discharge curves in Leclanché batteries and those predicted from theory based on a rigorous statistical thermodynamic approach to the solid phase redox system.

Assuming $MnOOH_r$ equivalent to a mixed oxide $(MnO_2)_{1-r} \cdot MnOOH_r$, Atlung obtained the relation:

$$E = E^\theta + RT/F \ln \frac{1-r}{r} \quad (2)$$

for the reduction $MnOOH_r + \delta H^+ + \delta e \rightarrow MnOOH_{r+\delta}$ where $0 < r < 1$ and $\delta \rightarrow 0$. The OCV plots of $E - E_{(\text{at } r=0.5)}$ vs r in Equation 2 showed large deviations from the observed curves. Treating MnO_2 as an insertion electrode, analogous to $Li\text{–}TiS_2$, it has been shown that:

$$E = E^\theta + 2RT/F \ln [(1-r)/r] \quad (3)$$

which gave good agreement for $r < 0.5$, but for $r > 0.5$ the agreement was not satisfactory. Atlung and Jacobsen, therefore, observed that as proton insertion proceeds in the MnO_2 lattice, for some reason or another, some of the unoccupied sites become inaccessible to proton insertion. Using a parameter α to account for the number of unavailable sites, the following relation has been derived

$$E = E^\theta + 2RT/F \ln \frac{[1-(1+\alpha)r]^{1+\alpha}}{r(1+\alpha r)^\alpha} \quad (4)$$

where $\alpha = 1/r_{max} - 1$, r_{max} being the value of r at the theoretical end of homogeneous reduction which is readily determined by inspection of the observed OCV curve. For $\alpha = 0$ Equation 4 reduces to Equation 3. It has been shown that Equation 4 gave excellent agreement with the observed OCV curve for IC_1 with the value of $\alpha = 0.25$ on the basis of $r_{max} = 0.8$, as the end product is believed to be Mn_5O_8. This is equivalent to the oxide composition $MnO_{1.6}$ in agreement with that of Bell and Huber [22]. In the work of Kozawa [27], OCV curves for the IC MnO_2 samples have been used to test the validity of Equation 4. Using $\alpha = 0.25$, IC_2 like IC_1 also gives excellent agreement with the observed values (Fig. 3). Slight deviations were, however, observed in the range $0.1 < r < 0.3$ for the other EMD samples IC_3, IC_4, IC_9 and IC_{10}. The above model shows wide deviations for the chemical manganese dioxides CMD, namely, IC_5, IC_8 and those synthesized in the present investigations,

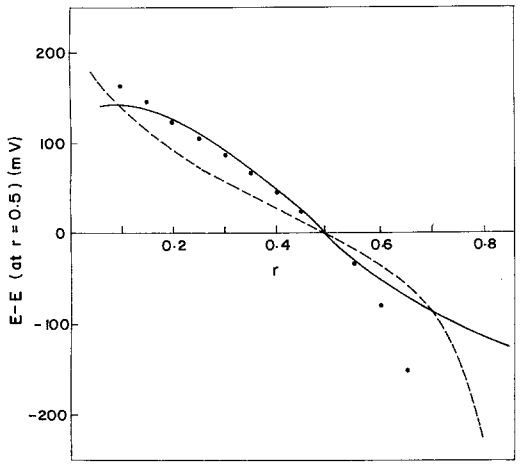

Fig. 4. Calculated and observed potential curves of IC_5; —— – observed, – – – – – calculated ($\alpha = 0.25$), ... – calculated ($\alpha = 0.47$).

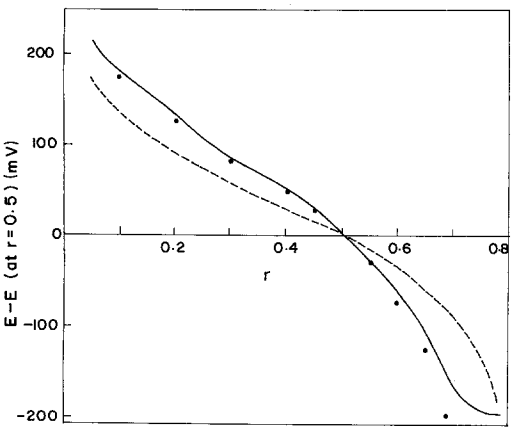

Fig. 6. Calculated and observed potential curve of A_5; —— – observed, – – – – – calculated ($\alpha = 0.25$), ... – calculated ($\alpha = 0.47$).

e.g. A_5, B_1 and B_2 (see Figs. 4–7). All these samples showed, however, an almost complete agreement with a value $\alpha = 0.47$ corresponding to $r_{max} = 0.68$. This value is justified by the nature of their observed OCV curves wherein a definite break is observed at that value in the latter*. This leads to another hypothesis: unlike the end product Mn_5O_8 for electrolytic manganese dioxides (EMDs) ($\alpha = 0.25$) the end product for the homogeneous phase reduction of CMDs could be different, i.e. Mn_3O_5 ($\alpha = 0.47$ or $r_{max} = 0.68$) equivalent to the oxide composition $MnO_{1.66}$. This means that the homogeneous phase reduction is over earlier for the CMDs. This again raises the ever puzzling question of whether the fundamental crystal structure of CMD and EMD is same (i.e. γ) or not (i.e. γ and/or ϵ). We have earlier suggested that the α- and γ-forms of CMD could be visualized to have been obtained via a structural transition, namely,

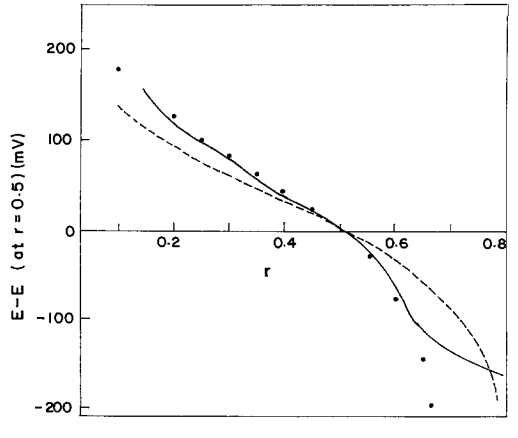

Fig. 5. Calculated and observed potential curve of IC_8; —— – observed, – – – – – calculated ($\alpha = 0.25$), ... – calculated ($\alpha = 0.47$).

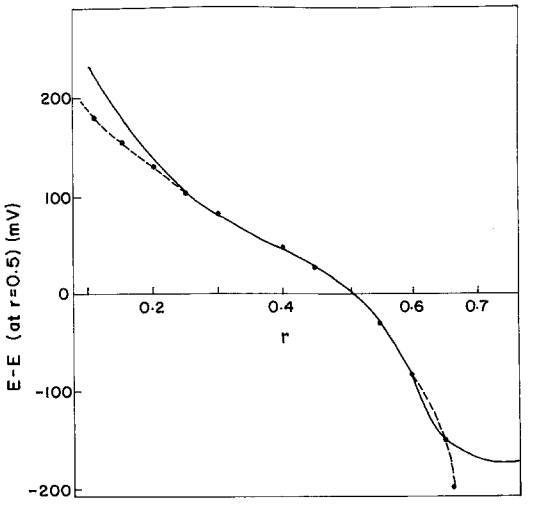

Fig. 7. Calculated and observed potential curves of B_1; —— – observed, ... – calculated ($\alpha = 0.47$), – – – – – calculated ($\alpha = 0.25$).

* The $E - E_{(at\ r=0.5)}$ shown in all the figures, i.e. from Fig. 3 to 11, are redrawn from the OCV curves only. These OCV curves, however, are not shown in Fig. 2.

$$\gamma \underset{\gamma \ldots\ldots \gamma, \alpha \ldots\ldots \alpha}{\rightleftharpoons} \alpha$$

Starting with an α-form, if γ-crystal phase is considered to be a limiting case of the structural transition under the specific conditions of preparation, then the existence of some residual α-domains or (2 x 2) tunnels in the γ-form is quite likely. If this assumption is valid, then it could imply the existence of some intergrown α-domains in CMDs analogous to pyrolusite domains in a ramsdellite matrix in EMD as proposed by de Wolff [23]. Voinov [24] has recently shown that an α-MnO_2 is the worst possible structure for the proton–electron insertion thus explaining its very poor electrochemical activity. The presence of some α-domains in chemical γ-MnO_2 could, therefore, be responsible for its relatively lower activity and a premature end to its homogeneous phase reduction, i.e. at $r = 0.68$ vs $r = 0.80$ for the EMD. That the increasing presence of the α-phase lowers the electrochemical activity of the γ-form and vice versa has been amply demonstrated in our earlier communication [11] i.e. w.r.t. the discharge curves of A_6, A_7 (α), A_1 (α, γ), A_4 (γ, α) and A_2, A_5 (γ), the discharge capacity increasing in that order. These observations appear to support the above hypothesis. To obtain a γ-CMD of high battery activity the factors favouring the formation of α-domains should, therefore, be carefully avoided during synthesis.

IC_{11}, a γ-MnO_2, shows a rather marked deviation between the theoretical potential curve

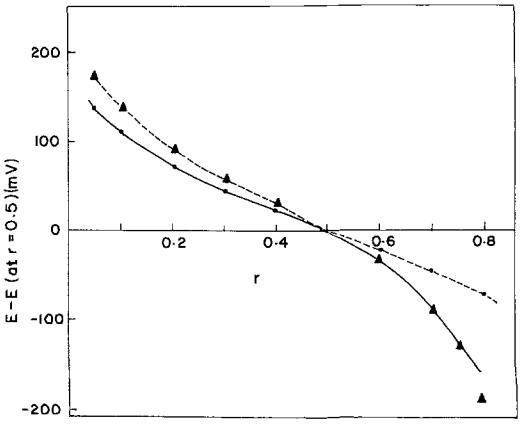

Fig. 8. Calculated and observed potential curves of IC_{11}; —— – observed, ... – calculated (α = 0), ▲▲▲▲ – calculated (α = 0.25), – – – – – calculated (α = 0.47).

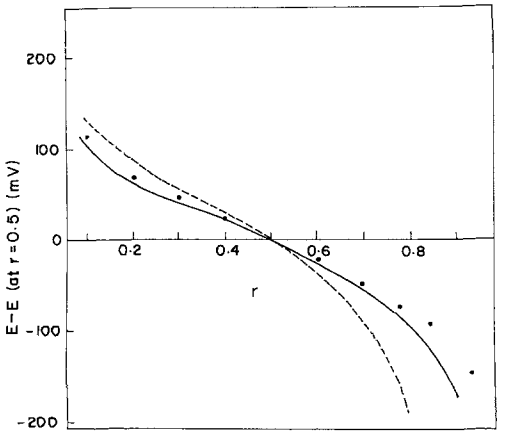

Fig. 9. Calculated and observed potential curves of a Ghana ore sample; —— observed, – – – – – calculated (α = 0.25), ... – calculated (α = 0).

and the experimental one. It shows two mechanisms for proton–electron filling of the MnO_2 lattice above and below $MnO_{1.75}$. In the first half it obeys Equation 3 but shows a substantial deviation in the second range, i.e. for $r > 0.05$ (Fig. 8). In the latter case, the use of $\alpha = 0.25$ in Equation 4 gives excellent agreement with the observed data. According to the reduction mechanism of Maskell, Shaw and Tye [15] and the Atlung-Jacobsen model [25] it appears that the proton insertion and/or electron delocalization is extremely favoured in the first half and the number of available sites for proton insertion decreases only in the second half of homogeneous phase reduction. It is interesting to note that for natural γ-MnO_2 (Ghana ore), $\alpha = 0$ in Equation 4 gave a much better agreement than $\alpha = 0.25$ (Fig. 9).

Samples C_3 and C_4 indicate that the homogeneous phase reduction extends only up to about $MnO_{1.70-1.75}$ (see Fig. 2). The Atlung–Jacobsen model, therefore, does not seem to be applicable to these two samples at least not over a major part of the reduction range. For C_3 (Fig. 10) the rate of fall of potential is appreciably greater than that expected from the $\alpha = 0.77$ curve.

The failure of Equation 4 to account for the observed potentials for these two samples, i.e. C_3 and C_4 could be due to the following:

(a) proton insertion is somehow hampered by the dopant and/or

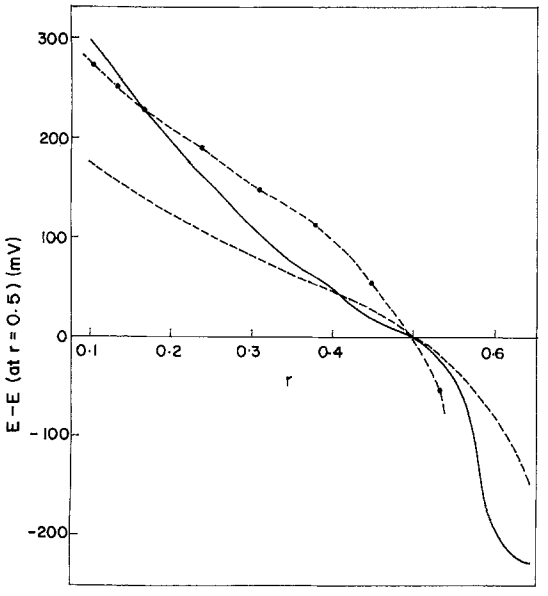

Fig. 10. Deviation of the observed potential curve from the calculated of C_3; —— – observed, – – – – – calculated ($\alpha = 0.25$), ... – calculated ($\alpha = 0.77$).

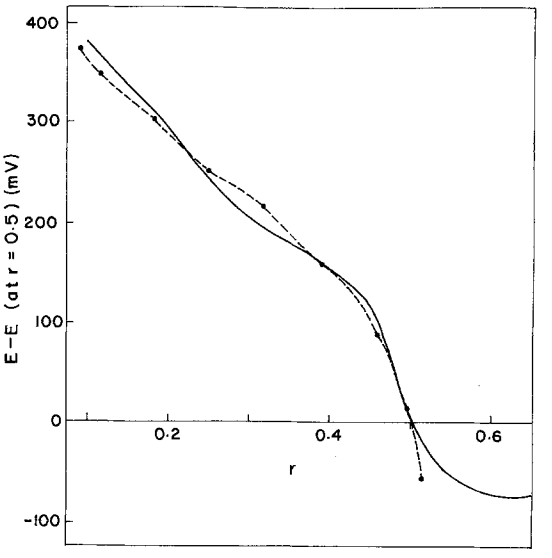

Fig. 11. Agreement between observed and theoretical potential curves of C_4 in the range $0 < r \leqslant 0.5$; —— – observed, ... – calculated ($\alpha = 0.88$).

(b) the influence of the electronic term μ_e^D as suggested by Atlung–Jacobsen [25] and Maskell, Shaw and Tye [15]

It is relevant to discuss here the location of Fe^{3+} in the γ-MnO_2 structure. The ionic radius of Fe^{3+} is 0.065 nm, similar to Mn^{3+}. An isomorphous substitution of Mn^{3+}, which is present in virgin MnO_2 by Fe^{3+}, seems quite feasible. Also, Fe^{3+} ions could substitute the octahedral sites occupied by Mn^{4+} (ionic radius 0.054 nm) and thus distort the regular octahedral structure as a result of the higher ionic radius of Fe^{3+}. An alternate view is to look at the γ-MnO_2 structure as a hexagonal close-packed structure in which Mn^{4+} ions and vacancies are distributed among the octahedral sites. In such a structure Fe^{3+} ions could easily substitute some Mn^{4+} ions. As a result of this the homogeneous phase reduction probably extends only up to that stage when the electron becomes delocalized between Fe^{3+} and Mn^{4+} octahedra, assuming that the two octahedra are alongside the octahedral double chains. What is more likely is that the electron is not in perfect resonance, but spends more time closer to one of the cations than the other. The relative electron affinities on the doped cations should then play an important role towards extending the homogeneous reduction range. It seems to be imperative that the doped cations be such that they are able to form stable oxyhydroxide compounds analogous to MnOOH during the reduction process. Cations such as Ti^{4+} or V^{5+} appear to be the likely candidates. It is puzzling, however, that the observed and the theoretical curves of Mo^{6+}-doped sample C_4 (Fig. 11) are in reasonably good agreement with each other, unlike those of C_3, suggesting thereby that Mo^{6+} is a 'better' dopant than Fe^{3+}.

It is strongly felt that high resolution transmission electron microscopy (HRTEM) along the X-ray photoelectron spectroscopy should yield valuable information regarding the location of dopants in the reduced structures. If this is coupled with X-ray diffractographic study of the discharge products at $r = 0.25$, 0.5, 0.75 and 1, it might make the investigation a little more comprehensive.

4. Conclusion

Manganese dioxides of very high catalytic activity are obtained by chlorate oxidation of Mn(II) salts containing Fe^{3+}. X-ray power diffraction data indicate that the presence of increasing

amounts of Fe^{3+} in the Mn(II) salt solutions favour the formation of the γ-phase of MnO_2. The presence of Fe^{3+} or MoO_3 in the crystal lattice of chemically precipitated manganese dioxides is detrimental to the discharge performance, contrary to some of the literature reports. Chemical γ-MnO_2 seems to be an intergrowth structure of the ramsdellite and pyrolusite structures along with some residual α-domains. The Atlung–Jacobsen model is apparently applicable for all $MnOOH_r$ systems, except doped CMDs, if an appropriate value of the parameter is chosen. In other words, MnO_2 seems to behave like an insertion electrode but the degree of insertion varies for EMD, CMD and natural manganese dioxide (NMD).

References

[1] J. P. Chevillot and J. P. Brenet, *C. R.* **249** (1959) 1869.
[2] P. Lancon, J. P. Chevillot and J. P. Brenet, *ibid.* **258** (1964) 6411.
[3] J. P. Brenet, in 'Batteries '2', Pergamon Press, Oxford (1965) 253.
[4] M. W. Rophael, T. A. Bibawy, L. B. Khalil and M. A. Malati, *Chem. Ind.* **1** (1979) 29.
[5] W. W. Mourad, M. W. Rophael and L. B. Khalil, *J. Appl. Electrochem.* **10** (1980) 309.
[6] B. P. Varma, J. Mukherjee and T. Banerjee, *Proc. Indian Natl. Sci. Acad. Part A* **41** (1975) 350.
[7] T. Väland, *J. Power Sources* **1** (1976) 65.
[8] J. B. Fernandes, PhD thesis, University of Bombay (1983).
[9] J. B. Fernandes, B. Desai and V. N. Kamat Dalal, *Electrochim. Acta* **28** (1983) 309.
[10] *Idem, ibid.* **29** (1984) 181.
[11] *Idem, ibid.* **29** (1984) 187.
[12] J. P. Brenet, K. Traore, M. Cyrankowska, G. Ritzler and R. Saka, Proceedings of the MnO_2 Symposium, Cleveland 1–2 October, 1975, Vol 1, Paper 14 (1975) pp. 264–288.
[13] J. P. Brenet, *Chimia* **23** (1969) 444.
[14] L. S. Dent-Glasser and L. Ingram, *Acta Cryst.* **B24** (1968) 1233.
[15] W. C. Maskell, J. E. A. Shaw and F. L. Tye, *Electrochim. Acta* **26** (1981) 1403.
[16] A. Kozawa and R. A. Powers, *J. Electrochem. Soc.* **113** (1966) 870.
[17] R. S. Johnson and W. C. Vosburgh, *ibid.* **100** (1953) 471.
[18] K. Newmann and E. V. Roda, *Zh. Elektrochem. Ber. Bunsenges. Phys. Chem.* **69** (1965) 347.
[19] F. L. Tye, *Electrochim. Acta* **21** (1976) 415.
[20] W. C. Maskell, J. E. A. Shaw and F. L. Tye, *ibid.* **28** (1983) 225.
[21] *Idem, ibid.* **28** (1983) 231.
[22] G. S. Bell and R. Huber, *J. Electrochem. Soc.* **111** (1964) 1.
[23] P. M. de Wolff, *Acta Cryst.* **12** (1959) 341.
[24] M. Voinov, *Electrochim. Acta* **27** (1982) 833.
[25] S. Atlung and T. Jacobsen, *ibid.* **26** (1981) 1447.
[26] H. Bizette, C. F. Squire and B. Tsai, *C. R.* **207** (1938) 449.
[27] A. Kozawa, Proceedings of the 11th International Symposium, 1978. 'Power Sources 7', (edited by J. Thompson) [Paper 30, p. 485] Academic Press, London (1979).